Suppression of the zero-order term in off-axis digital holography through nonlinear filtering

Nicolas Pavillon,[1,*] Chandra Sekhar Seelamantula,[2] Jonas Kühn,[1,3] Michael Unser,[4] and Christian Depeursinge[1]

[1]Advanced Photonics Laboratory, Ecole Polytechnique Fédérale de Lausanne (EPFL), CH-1015 Lausanne, Switzerland

[2]Department of Electrical Engineering, Indian Institute of Science, Bangalore, India

[3]Département de Psychiatrie-CHUV, Site de Cery, 1008 Prilly, Lausanne, Switzerland

[4]Biomedical Imaging Group, Ecole Polytechnique Fédérale de Lausanne (EPFL), CH-1015 Lausanne, Switzerland

*Corresponding author: nicolas.pavillon@a3.epfl.ch

Received 21 September 2009; revised 21 October 2009; accepted 22 October 2009; posted 23 October 2009 (Doc. ID 117098); published 9 November 2009

We present experimental validation of a new reconstruction method for off-axis digital holographic microscopy (DHM). This method effectively suppresses the object autocorrelation, namely, the zero-order term, from holographic data, thereby improving the reconstruction bandwidth of complex wavefronts. The algorithm is based on nonlinear filtering and can be applied to standard DHM setups with realistic recording conditions. We study the robustness of the technique under different experimental configurations, and quantitatively demonstrate its enhancement capabilities on phase signals.

OCIS codes: 090.1995, 100.2000, 100.3010, 100.3175, 120.5050, 180.3170.

1. Introduction

In a previous publication [1] we proposed a new method to suppress the zero-order term in digital holographic reconstruction. This technique suppresses the requirement of having a separation constraint between the zero-order and the diffraction terms, thereby extending the available spectral support of the image. We showed that the proposed technique suppresses the zero-order term under realistic conditions. Here we address the robustness of the method under some practical conditions and present experimental results that demonstrate the suppression of the artifacts generated by the zero-order term. We then show the quantitative improvement on the phase signal.

During the past few decades, digital holographic microscopy (DHM) has evolved significantly, thanks to the availability of charged-coupled device (CCD) cameras and fast computers. From the first digital developments [2] to digital complex wave measurements [3,4], this technology led to many different applications such as profilometry [5] and biological investigation [6,7], where the quantitative phase signal can be linked to biological parameters. Several publications study in detail the imaging process of DHM [8,9]; a comprehensive study of the imaging process in Fresnel holography was presented recently [10].

Since the discovery of holography by Gabor [11], the fact that three different contributions of the diffracted beam are generated from the hologram, namely, the zero-order term, the +1 and −1 diffraction orders, i.e., real and conjugated images, had to be addressed. Since these terms are superimposed in the recorded signal, the complex image is altered

0003-6935/09/34H186-10$15.00/0

by other contributions. The methods proposed to address this problem fall into two main categories:

i. (i) Modulation of the signal; it spatially separates the different terms contained in the hologram [12]. This approach leads to spatial filtering and so-called Fourier methods [13,14] in the off-axis configuration.

ii. (ii) Temporal phase-shifting interferometry (PSI); it relies on combinations of several holograms in the case of inline measurements [15].

Phase shifting is classically done with a four-step or a three-step algorithm [16]. However, these methods need accurate and equally spaced phase shifts that require expensive devices. More recently, adaptive PSI was investigated, making it possible to use holograms without accurately known phase shifts [17,18], at the cost of employing iterative procedures. Recent developments demonstrated that it is also possible to recover the complex field from only two interferograms [19,20].

One of the main features of off-axis DHM is that one can recover the complex signal with one acquisition only. However, while the spatial separation between the two conjugate images is usually fulfilled, there could be overlap between the diffraction terms and the zero-order terms, leading to a loss of signal quality.

Different methods were proposed to specifically suppress the zero-order term. Although high-pass filtering together with spatial windowing has proved to be efficient [21,22], it has the drawback of altering the reconstructed signal because of the global filtering effect. In analogy to standard PSI methods, phase shifting applied in the spatial domain has also been used for off-axis DHM [23,24]. These techniques, however, suffer from the limitation that they require the variations of the signal to be slow relative to the fringe pattern. Other specific methods have also been developed, such as subtraction holography, which uses the speckle pattern of the object [25]; they are nevertheless not directly applicable to DHM because of the differences in the type of measured signal.

Recently, a numerical approach based on a linear approximation of the interference equation was proposed [26]; this technique, however, is applicable only to amplitude objects with an inline configuration and with a plane wave reference whose phase is precisely controlled. A method based on the use of the logarithm operator, somewhat similar to the technique proposed in this article, was investigated in 2004 for inline holograms [27]. This algorithm is based on neglecting the object intensity contribution when the reference intensity is strong in comparison, enabling PSI reconstruction with only two acquisitions. It was also shown recently that wavelets could be used for zero-order suppression [28].

The method presented here is based on nonlinear filtering and can be applied to off-axis DHM. It has no restrictive requirements on the object or on the reference. The two main conditions are that the reference amplitude must be stronger than that of the object and that the desired imaging order must be confined to one quadrant of the Fourier domain. Apart from these conditions, which can be easily fulfilled in practice, the method is general. It is noniterative and its computational cost is moderate.

In Section 2 we briefly recall the theoretical aspects, with emphasis on the experimental consequences of the assumptions. We also demonstrate that the proposed method can provide diffraction-limited reconstruction in off-axis DHM. In Section 3 we first present experimental results and address practical issues such as the quality of the reference or the importance of the intensity ratio between the reference and the object waves. Finally, we quantify the improvement on the phase signal through the proposed method.

2. Theory

A. Hologram Reconstruction

Complex wavefront reconstruction in off-axis DHM has been extensively described, for example, in [8,29]. We hereby recall only the basic principles and necessary elements to characterize the performance of the new technique and compare it with standard Fourier methods. For the sake of simplicity, we limit our analysis to the equations in the continuous domain.

The interference pattern recorded on the camera plane is

$$\begin{aligned} i(x,y) &= |r(x,y)+o(x,y)|^2 \\ &= |o(x,y)|^2+|r(x,y)|^2+o(x,y)^*r(x,y) \\ &\quad + o(x,y)r(x,y)^*, \end{aligned} \tag{1}$$

where $o(x,y)$ is the object wave, $r(x,y)$ is the reference wave, and the asterisk denotes the complex conjugate operator. The first two terms of Eq. (1) correspond to the so-called zero-order term; the last two terms are the $+1$ and -1 diffraction orders, which are the real and virtual images, respectively. Using different propagation directions for the two interfering waves modulates the diffraction terms at a carrier spatial frequency, so that they do not overlap spectrally; it thus makes it possible to filter one of the imaging orders by Fourier techniques (FTs) [30]. In this case the object wavefront is given by

$$\begin{aligned} o^{\mathrm{FT}}(x,y) &= r_D(x,y)i_F(x,y), \\ i_F(x,y) &= \mathcal{F}^{-1}\{\mathcal{F}\{i(x,y)\}W(\omega_x,\omega_y)\}, \end{aligned} \tag{2}$$

where $W(\omega_x,\omega_y)$ is the filtering window function in the frequency domain, and $i_F(x,y)$ is the filtered hologram; r_D is a digital reference wave classically taken as the complex conjugate of the reference wave used during the experiment. The wavefront can then be numerically reconstructed by digital Fresnel propagation. In this case, the in-focus complex wavefront becomes [9,31]

$$\Psi(x,y) = A\frac{\exp(2\pi i d/\lambda)}{i\lambda d}\mathcal{F}^{-1}\{\mathcal{F}\{r_D(x,y)i_F(x,y)\}G(\omega_x,\omega_y)\}, \qquad G(\omega_x,\omega_y) = \exp\{-i\pi\lambda d[\omega_x^2+\omega_y^2]\}, \tag{3}$$

where A is a real constant, $i = \sqrt{-1}$, λ is the source wavelength, and d is the reconstruction distance, which is equal to the distance between the recording plane and the in-focus image; $G(\omega_x,\omega_y)$ is the convolution kernel of the Fresnel transform in the reciprocal domain. Note that the direct implementation of the Fresnel transform introduces numerical artifacts that are due to periodization effects; they can be reduced by apodizing the borders of the hologram [32].

B. Principle of the Nonlinear Technique

The detailed derivations and description of the algorithm are given in [1]; here we recall only the primary elements.

By rearranging the terms in Eq. (1) (spatial coordinates are omitted for the sake of brevity), we obtain

$$\frac{i}{|r|^2} = \left(1+\frac{o}{r}\right)\left(1+\left(\frac{o}{r}\right)^*\right). \tag{4}$$

Next we take the logarithm

$$\ln\left(\frac{i}{|r|^2}\right) = \ln\left(1+\frac{o}{r}\right) + \ln\left(1+\left(\frac{o}{r}\right)^*\right), \tag{5}$$

which transforms the product into a sum, allowing for the subsequent separation of the interference terms from the zero-order term. We have shown [1] that if the reference amplitude is higher than that of the object wave, and if the imaging order is confined in one quadrant of the Fourier spectrum, the terms on the right-hand side of Eq. (5) have their spectra contained in the same quadrant as the usual imaging orders o^*r and or^*. As a result, the two terms can be filtered out spectrally. The first assumption is required to guarantee the stability of the algorithm; the second one ensures the possibility of recovering the desired image by Fourier filtering. It is therefore feasible to retain the desired imaging order by selecting the corresponding quadrant of the hologram spectrum. The signal is then recovered by inverse Fourier transformation. The filtered diffraction order in the spatial domain is given by

$$\begin{aligned} i'_F(x,y) &= \ln\left(1+\frac{o}{r}\right) \\ &= \mathcal{F}^{-1}\left\{\mathcal{F}\left\{\ln\left(\frac{i}{|r|^2}\right)\right\} \times \mathbf{1}_{[0,\infty)\times[0,\infty)}\right\}, \end{aligned} \tag{6}$$

where the indicator function $\mathbf{1}_{[0,\infty)\times[0,\infty)}$ denotes the window used to select the relevant quadrant (in this particular case, the first quadrant). Ultimately, the recovered object wavefront in the hologram plane is given by

$$o^{\mathrm{NL}}(x,y) = r_D(x,y)(\exp(i'_F(x,y)) - 1), \tag{7}$$

which specifies our nonlinear (NL) filtering method .

By comparing Eq. (2) with Eqs. (6) and (7), we find that the proposed algorithm is similar to the standard Fourier filtering method, except for the nonlinear logarithm and exponential operations. The object complex wavefront is reconstructed by multiplying the filtered signal with a digital reference wave, as in standard off-axis DHM, and by digitally propagating to obtain the in-focus image, as described in Subsection 2.A. One can note that Eq. (6) is slightly similar to the development given in [27]. However, the theoretical background and hypothesis implied are different, since our proposed method is limited to off-axis geometry but does not require any approximations on interference Eq. (1).

The new technique just presented requires some specific conditions to be satisfied during hologram recording. The first condition, namely, $|r| \gg |o|$, is usually readily fulfilled in a global sense, since it was shown that higher intensity in the reference wave yields a better signal-to-noise ratio (SNR) of the phase signal [33]. This condition cannot be fulfilled for every pixel in the hologram plane, particularly in the case of out-of-focus images, which could contain strong intensity regions, mainly induced by the highly diffracting parts of the sample.

It is also required that the spectra of the $+1$ and -1 diffraction orders do not overlap. This condition is naturally fulfilled in the case of off-axis DHM. Confining the usable frequency space to one specific quadrant is equivalent to having interference fringes inclined at 45°, which corresponds to ideal measurement conditions, i.e., the best spatial sampling case for those high frequencies. Moreover, as can be seen from Eq. (6), prior knowledge of the reference intensity is required, since our algorithm suppresses the object zero-order term, i.e., $|o|^2$, but not $|r|^2$. It corresponds in fact to a subtraction of $|r|^2$ before processing.

It should be noted that the reference is commonly assumed to be a plane wave, so that elimination of its intensity corresponds to simply subtracting a constant. However, some wavefront aberrations are always present in practice, which induce irregularities in the reconstructed signal. Furthermore, while the object spectrum is limited by the cutoff frequency of the microscope objective (MO), the reference wave can have a larger spatial spectral support. Nevertheless, our experimental results show that it is possible to counter those effects by simple subtraction of a reference intensity that is recorded during a calibration step.

C. Comparison with Fourier Filtering Techniques

There are two well-established techniques for suppressing the zero-order term. The first is to consider the reference intensity as a dc term that could be suppressed by subtracting the mean value of the hologram [21]. The other is to use high-pass (HP) filtering before processing the hologram to attenuate the zero-order term, seen as a low frequency term, while keeping the spatially modulated components, namely, the imaging terms [22].

A high-pass filtered version of the hologram can be obtained by subtracting a low-pass filtered component from the original signal:

$$i^{\mathrm{HP}} = i - i * h_k, \qquad h_k(m,n) = \frac{1}{k^2}, \quad \forall\ |m,n| < \frac{k}{2}, \tag{8}$$

where $*$ is the convolution operator and $h_k(m,n)$ is a low-pass filter consisting in a normalized matrix of size $k \times k$.

To demonstrate the effect of this type of filter, we selected two high-pass kernels, with, respectively, $k = 3$ and $k = 7$. The frequency response of those filters is shown in Fig. 1, where the positions of the interference terms are shown for the experimental case presented in Subsection 3.C. As is shown in Fig. 1, the high-pass filters have a strong attenuation in the low frequency region and ripples at higher frequencies. Consequently, the zero-order term is strongly attenuated, but phase artifacts arise in the imaging terms since the response is not necessarily symmetric around the modulation frequency.

D. Diffraction-Limited Imaging in Off-Axis Digital Holographic Microscopy

It is common to consider that part of the spatial resolution is lost in the case of off-axis DHM because a significant portion of the spectral bandwidth is occupied by the unused terms of Eq. (1), as presented in Fig. 2(a). We show here that diffraction-limited imaging is made possible for off-axis DHM if the zero-order term is properly suppressed by allowing the use of a larger bandwidth for diffraction orders.

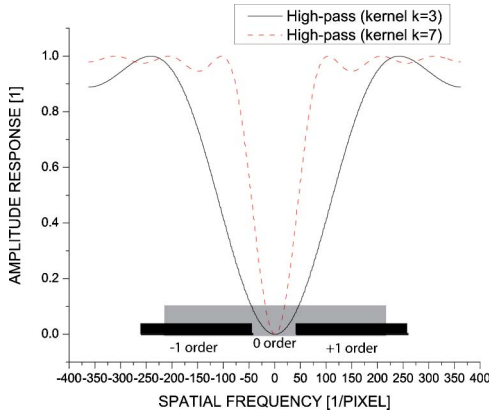

Fig. 1. (Color online) Frequency response of the high-pass filters corresponding to different kernel sizes as defined in Eq. (8). The position of the interference terms is shown, corresponding to the experimental results in Subsection 3.C.

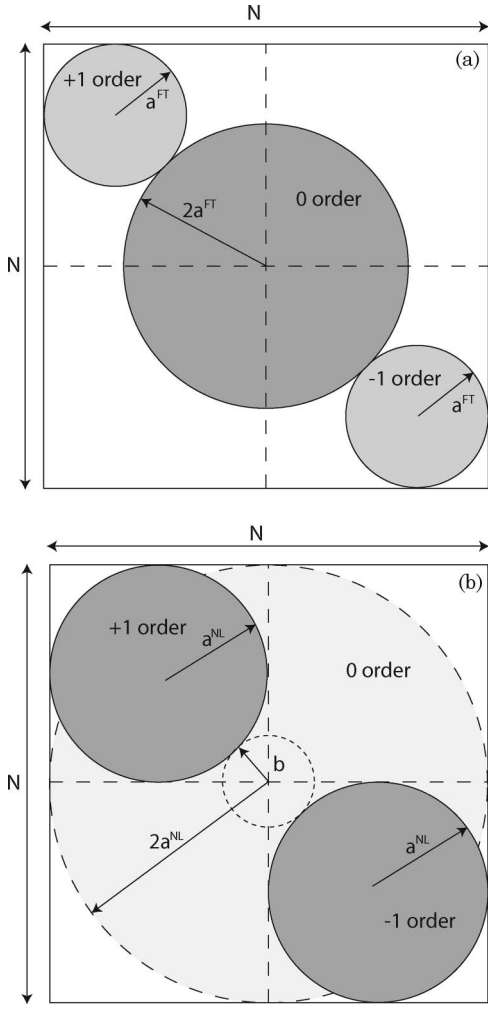

Fig. 2. Optimal spectral configuration of the Fourier transform of a hologram in the case of (a) Fourier technique (FT) and (b) nonlinear (NL) reconstruction with object autocorrelation suppressed, improving the usable bandwidth for the imaging order.

If we consider an object whose discrete spectral support is a circle of radius a, the optimal placement of the components in the hologram spectrum would look like the one shown in Fig. 2(a). We assume a squared recording zone of $N \times N$ pixels, with uniform sampling, and with identical interpixel distance along both axes, i.e., $\Delta x = \Delta y$.

For simplicity, we consider a plane wave reference whose spectrum is a two-dimensonal Dirac distribution $\delta(\omega_x, \omega_y)$, where ω_x and ω_y are the spatial frequency variables. The fact of choosing a plane wave makes it possible to neglect the influence of the reference intensity, which can be subtracted in practice. The term $|o|^2$ is the autocorrelation $(\mathcal{F}\{o\} * \mathcal{F}\{o^*\})$ of the Fourier transform of the object wave and therefore has a spectral radius of $2a$. On the other hand, the two diffraction terms are the convolution of the Fourier transform of the object with δ and therefore have the same discrete radius a.

From geometric considerations it can be seen that the maximal spatial bandwidth achievable with linear Fourier reconstruction methods is given by

$$a_{\max}^{\mathrm{FT}} = \frac{N}{2+3\sqrt{2}}. \tag{9}$$

On the other hand, the proposed nonlinear technique requires that diffraction orders are confined in one quadrant of the frequency plane [see Fig. 2(b)]. Thus, the maximal frequency allowable in the nonlinear case reconstruction is

$$a_{\max}^{\mathrm{NL}} = \frac{N}{4}, \tag{10}$$

which is approximately 1.5 times larger than $a_{\max}^{\mathrm{FT}}$. In the case of a circular support, the central portion of the spectrum near the origin will never be filled with frequencies, which can be expressed as a circle of radius [see Fig. 2(b)]:

$$b = \left(\sqrt{2}-1\right)a^{\mathrm{NL}}. \tag{11}$$

Considering a circular support for the Fourier transform of the object is justified by the fact that, in microscopy, the highest reachable frequency is limited by the numerical aperture (NA) of the MO, defined as $\mathrm{NA} = n_i \sin(\alpha)$, where n_i is the refractive index of the surrounding medium and α is the maximal half-angle that can be detected. The spatial cutoff frequency of the objective can be calculated as follows:

$$p^{\mathrm{MO}} = \frac{\sin(\alpha)}{\lambda} = \frac{\mathrm{NA}}{n_i \lambda}, \tag{12}$$

which is the standard equation to determine the resolution of an optical system. The discrete spectral support can then be related to the continuous one as

$$a^{\mathrm{MO}} = \frac{\mathrm{NA}}{n_i \lambda}\frac{N\Delta x}{M}, \tag{13}$$

where M is the magnification. a^{MO} corresponds therefore to the discrete spatial bandwidth of the MO; $a_{\max}^{\mathrm{FT}}$ and $a_{\max}^{\mathrm{NL}}$ correspond to the maximal usable bandwidth where no overlap between the interference terms occurs for the standard and nonlinear reconstruction techniques, respectively.

The discrete bandwidths $a_{\max}^{\mathrm{FT}}$, $a_{\max}^{\mathrm{NL}}$, and a^{MO} have been calculated according to their definitions. These calculations are made for standard MOs whose specifications are listed in Table 1 for an acquisition device and laser wavelength identical to the ones used during the experiments ($\Delta x = 6.45\,\mu\mathrm{m}$ and $\lambda = 680\,\mathrm{nm}$). The calculations are presented in Fig. 3, where all the values have been normalized by N to make them independent of the image size. Those results show that, theoretically, the standard reconstruction requires a magnification factor of 40× to avoid resolution limitation, whereas the new method can provide diffraction-limited imaging conditions all the way down to 4× magnification.

Table 1. Specifications of the MOs Used for the Calculations of Fig. 3

Magnification	4×	10×	20×	40×	63×	100×
NA	0.10	0.25	0.40	0.65	0.85	1.25
Immersion	Air	Air	Air	Air	Air	Oil
Refractive index n_i	1	1	1	1	1	1.518

One should note that the chosen range used for Fig. 3 represents only one type of MO. Typically, the use of immersion objectives increases the NA while maintaining constant magnification. This implies that objectives of 40× or 63× magnification would not reach diffraction-limited imaging conditions for standard reconstruction when using an immersion medium. Furthermore, although the development presented above was made for red light ($\lambda = 680\,\mathrm{nm}$), it can be considered as valid for a broader spectrum. Since CCD cameras with a pixel size of $\Delta x = 4\,\mu\mathrm{m}$ are currently commercially available, the ratio $\Delta x/\lambda$ in Eq. (13) can be kept constant or lower also for blue light ($\lambda = 480\,\mathrm{nm}$), so that the results presented in this section are valid for the whole visible range when employing proper devices.

As can be seen in Fig. 2(b), the proposed method can be automated easily. In the case of spatial filtering, the window must be chosen manually, since it is usually difficult to automatically determine the important spectral components for reconstruction. In the case of the nonlinear technique, the relevant quadrant can be easily selected by locating the maxima in the Fourier plane, for example.

3. Experiments and Discussion

Here we demonstrate the capability of the proposed method through different experiments. First, in Subsection 3.B we present the capability of the nonlinear method for reconstruction without filtering. Then we show the improvements on details of the

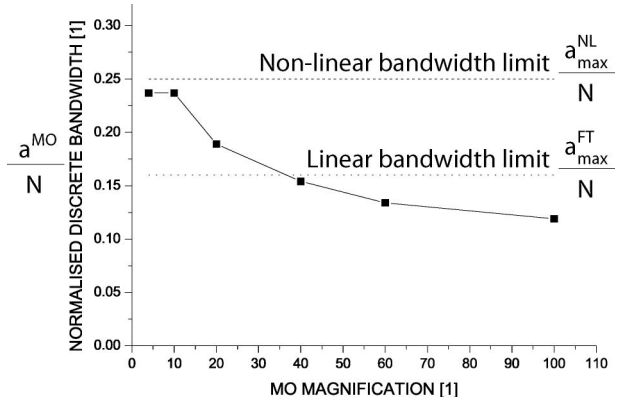

Fig. 3. MO normalized discrete spatial bandwidth a^{MO}/N in comparison with the maximal available bandwidth for standard ($a_{\max}^{\mathrm{FT}}/N$) and nonlinear ($a_{\max}^{\mathrm{NL}}/N$) reconstruction techniques.

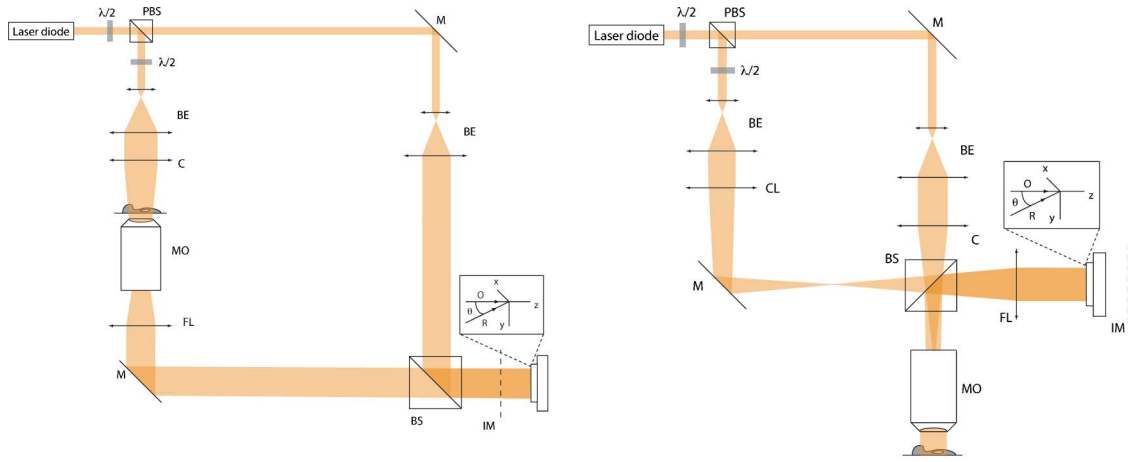

Fig. 4. (Color online) Optical sketch of the (a) transmission and (b) reflection holographic microscopes. (P)BS, (polarizing) beam splitter; $\lambda/2$, half-wave plate; M, mirror; BE, beam expander; C, condenser lens; MO, microscope objective; FL, field lens; IM, image plane; CL, curvature lens.

reconstructed image when employing optimal reconstruction parameters. Finally, in Subsection 3.C we quantify the potential improvement on the phase signal.

A. Experimental Setups

We took measurements of state-of-the-art transmission and reflection DHM setups [8], which are shown in Figs. 4(a) and 4(b), respectively. In transmission, the sample is illuminated with a laser diode ($\lambda = 680\,\text{nm}$), and an image is formed at plane IM, so that the signal can be recorded in the Fresnel domain with an 8 bit monochrome CCD camera (Basler A102f, pixel size: $\Delta x = 6.45\,\mu\text{m}$) with an employed field of view of 512×512 pixels and an exposure time of approximately 1 ms. In the reflection configuration, the wavelength of the source is $\lambda = 657\,\text{nm}$; all the other experimental parameters are identical to that of the transmission configuration. The intensity ratio between reference and object waves can be controlled with polarization optics and, before measurements were taken, was systematically checked by comparing an image of the object beam with that of the reference beam alone.

B. Experiment with a Phase Object

We imaged a solution of yew pollen cells in water in the transmission configuration with a 10× MO (0.25 NA). We chose a low magnification to ensure that some spectral overlap occurs between the imaging order and the zero-order term, as presented in Subsection 2.D. The hologram was recorded in the Fresnel domain, corresponding to a reconstruction distance of $d = 4.85\,\text{cm}$.

The mean intensity ratio between the reference and the object waves, computed as

$$\mu = \frac{\bar{I}_r(x,y)}{\bar{I}_o(x,y)}, \tag{14}$$

is 21.88, whereas the minimum is 2.21. This big difference is due to strongly diffracting points, so that the reference intensity must be high enough to ensure that the intensity condition is fulfilled at each pixel. The condition derived in Subsection 2.B was related to amplitude of fields ($|r| \gg |o|$) but is applied in practice to intensities. This is justified by the fact that the two conditions are equivalent.

The hologram was reconstructed by filtering one quadrant of the Fourier plane with the standard linear Fourier method and the proposed nonlinear method. The results are presented in Fig. 5, where one can see the strong influence of the zero-order term in the case of the linear method [see Fig. 5(a)], whereas a strong part of this parasitic term has been suppressed by using the nonlinear method [see Fig. 5(b)]. Although a significant amount of the dc term has been suppressed, an important part is still present, which corresponds to the reference intensity term $|r^2|$. As can be seen in Fig. 5(b), this term is not constant, which shows that the approximation made in considering it as a plane wave is not appropriate for proper suppression of the reference intensity term. The reconstruction with nonlinear filtering and reference subtraction is shown in Fig. 5(c), where the dc component of the hologram was also suppressed, i.e., the spectral component at the origin. In this case, one can see that the zero-order term is fully suppressed.

The selected quadrant of the hologram spectrum is shown in Fig. 6 for the two methods, where it is possible to identify the overlap of frequencies between the zero-order term and the imaging order for linear filtering [see Fig. 6(a)]. On the other hand, the nonlinear method suppresses the zero-order term [see Fig. 6(b)], so that frequency energy near the origin reaches back to the noise level, so that is possible to identify the spatial cutoff frequency of the MO around the whole circumference.

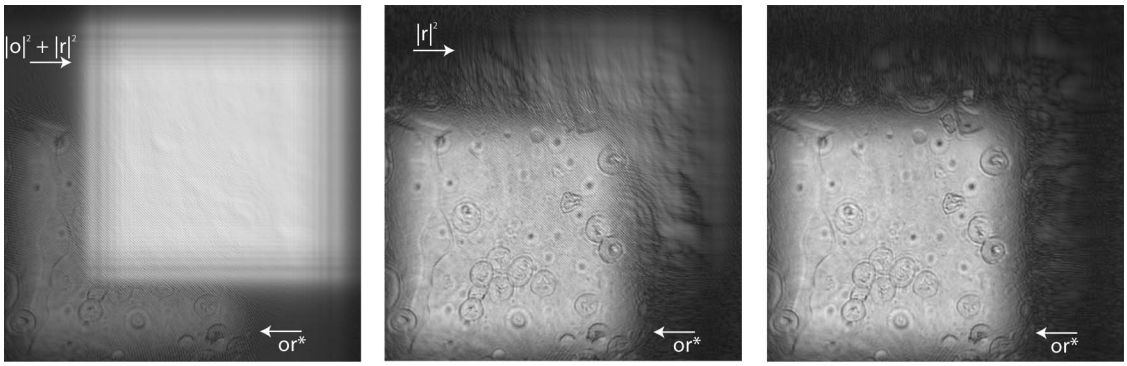

(a) (b) (c)

Fig. 5. Solution of yew pollens reconstructed with (a) the linear Fourier technique with the full zero-order term, (b) the nonlinear technique with the reference intensity term, and (c) the nonlinear technique with subtraction of the experimental reference and mean suppressed, where the zero-order term is suppressed (contrast in each image is scaled independently on full dynamic range)

One must observe that, despite the subtraction of the residual $|r|^2$ term, some spectral components are still present in the vicinity of the origin even for the nonlinear case. These components are due to some differences between the reference intensity recorded for subtraction and the one used during the hologram generation due to experimental noise, such as vibrations of the experimental setup or shot noise.

In our experiment, we blocked the object beam manually, implying that a delay in the range of seconds occurs between the measurements of the hologram and the one of the reference intensity. To minimize the variations on reference intensity, one can use an automatic shutter so that the two measurements could be performed with delays typically in the millisecond range, minimizing the effects of vibrations. Moreover, to minimize the effects that are due to shot noise, temporal averaging could be used during the calibration step by acquiring several images of the reference intensity. Then, another effect causing part of the residual components is the discretization of the hologram. Fringes in the hologram plane are sampled by the pixels, implying that part of the information about the object is lost, inducing reconstruction errors.

The same hologram was reconstructed by using the method employed for Fig. 5(c) and by keeping only the spatial region containing the imaging order,

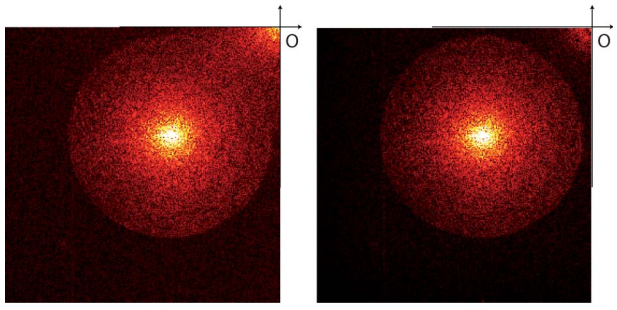

(a) (b)

Fig. 6. (Color online) Relevant quadrant of the yew pollen cells hologram spectrum after (a) linear Fourier filtering and (b) the nonlinear method.

making it possible to estimate the improvement provided by the proposed method in finer detail, as shown in Fig. 7. The linear method [Figs. 7(a) and 7(b)] and the nonlinear technique [Figs. 7(c) and 7(d)] are shown in amplitude and phase, respectively. The zero-order effect can be identified as a parasitic high-frequency term in a region of the images; this is due to the fact that, after demodulation of the off-axis hologram, the dc component becomes an ac term, i.e., is modulated. Those high frequencies are efficiently suppressed in the case of the nonlinear filtering method as shown in the insets of Fig. 7.

Although the zero-order term is efficiently suppressed through the proposed nonlinear filtering approach, some small remnants of high frequencies can be identified in the reconstruction shown in Fig. 7(d). Those strong components are indeed not fully suppressed, because the approximations made in the theoretical analysis are not exactly satisfied. However, as will be shown in Subsection 3.C, those strong frequencies are situated at the origin, where no overlap occurs between the zero-order term and the imaging term, so that they can be filtered out by using, for example, a Fourier mask computed with Eq. (11). This filtering was not done for the results shown in Fig. 7 to demonstrate the intrinsic performance of the proposed method.

C. Influence of the Intensity Ratio

In Subsection 3.B, we demonstrated qualitatively the efficiency of the proposed technique. Here we quantify the improvement in phase image quality provided by the nonlinear technique when there is overlap between the zero-order term and the diffraction order. The specimen is a mirror with a scratch, measured in reflection with a 20× MO (0.4 NA). The scratch introduces strong directional frequencies that overlap with the diffraction order, as shown in Fig. 8. Those components create artifacts in the amplitude, which can be seen at the bottom right of the image [see the dashed region in Fig. 9(a)]. Although they cannot be readily identified in the phase image [see Fig. 9(b)], those artifacts are also present. The

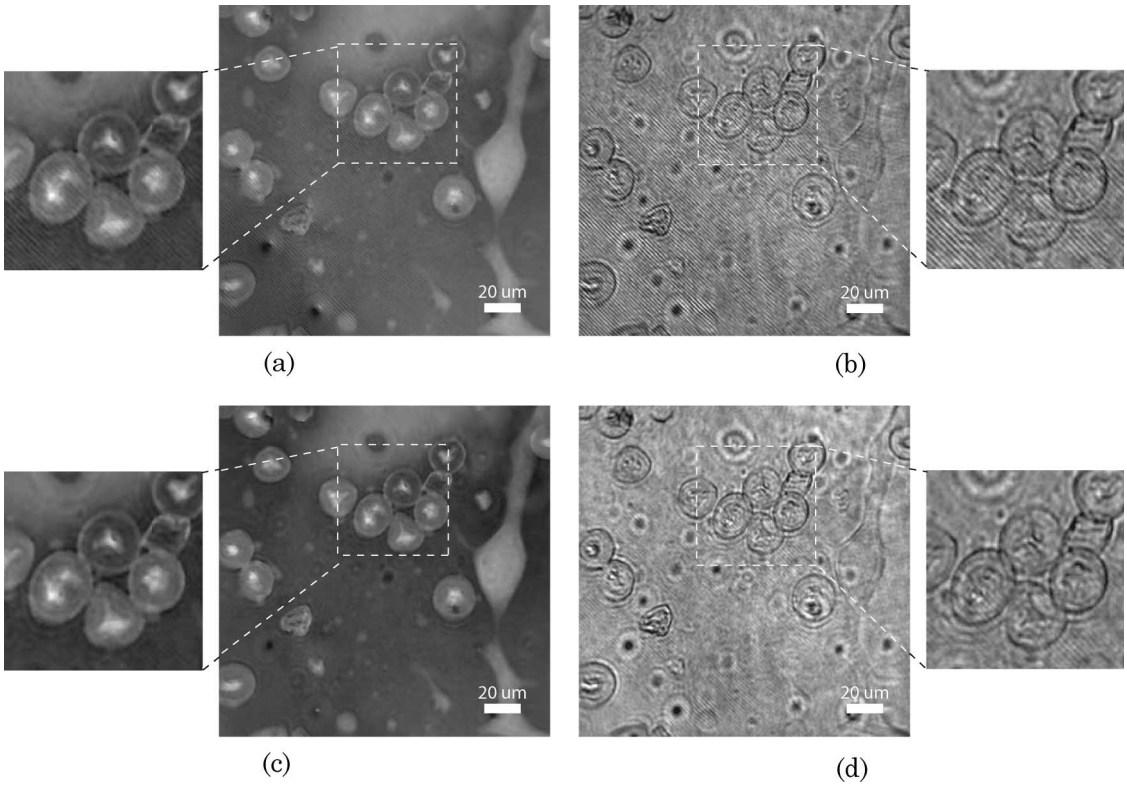

Fig. 7. Specimen solution of yew pollen cells. Reconstruction with (a),(b) the linear Fourier technique and (c),(d) the nonlinear method with (a),(c) comparison in phase and (b),(d) amplitude. Insets show a part of the field of view (contrast scaled independently on full dynamic range).

mean intensity ratio of the presented hologram is $\mu = 1.7$, and the images were obtained with a propagation distance of $d = 4.3\,\mathrm{cm}$. The reconstruction made with the linear Fourier method highlights these artifacts.

To make a fair comparison between the two techniques, the measured reference intensity was subtracted in all cases to account for the $|r|^2$ term. All the holograms were spatially filtered before propagation with the same circular mask at the origin, so that only the overlapping zero-order term is considered (see the dashed circle in Fig. 8). The radius of the circle was computed according to Eq. (11), where the numerical bandwidth is measured as $a^{\mathrm{MO}} = 105$ pixels; correspondingly b was taken as 42 pixels.

The phase standard deviation is computed in a 200 pixel square zone shown in Fig. 9(b) for different intensity ratios [defined by Eq. (14)] between the reference and the object waves. The results are shown in Fig. 10, where the standard deviation values were fitted with a fourth-order polynomial to show the main trend of the curve. One can identify that, for the two reconstruction techniques, the standard deviation seems to have a minimum in the middle of the intensity ratio values. The higher standard deviations at low ratios are due to the fact that the phase is distorted by the spectral power of the zero-order term, which depends directly on the power of the object wave. On the other hand, one can assume that, for high intensity ratios, the amount of available photons in the object wave decreases, leading to higher standard deviations that are due to the increase of the influence of shot noise. This implies that there is an optimum for the phase SNR, which corresponds to a reference wave intensity comprised approximately between 75% and 90% of the total power. This result is in agreement with previously published studies on SNR of phase signals [33].

In the case of the nonlinear filtering technique, the standard deviation is rather high for low intensities, since the assumption of the reference wave being stronger than the object is not fulfilled. Then

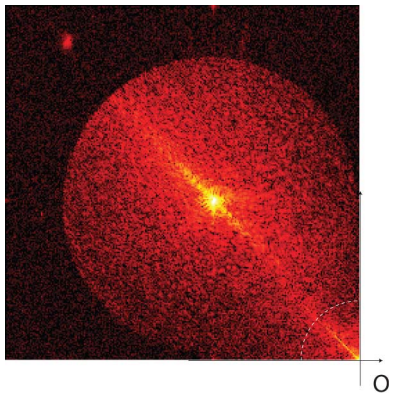

Fig. 8. (Color online) Magnitude of a quadrant of the Fourier transform of the hologram of the mirror scratch. The dashed circle shows the region of the spectrum that is spatially filtered.

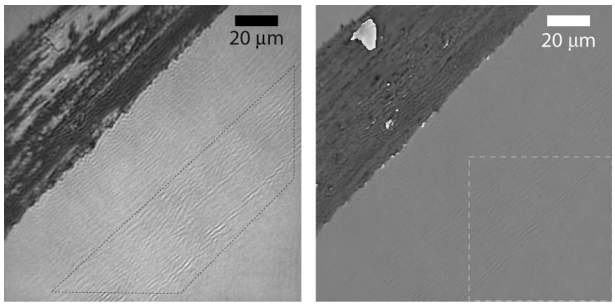

Fig. 9. Specimen mirror with a scratch (a) amplitude and (b) phase reconstructed with the standard linear technique. The black dashed square in (a) shows the artifacts induced by the zero-order term in amplitude. The white dashed square in (b) shows the region in the phase image where the standard deviation is computed.

it rapidly reaches a minimum at a mean intensity ratio of 5 and stays at a standard deviation of approximately 2°. The quantitative analysis also makes it possible to compare the proposed nonlinear technique with the high-pass filters defined in Subsection 2.C. The same procedure as described above was applied for reconstructions, where the hologram was previously filtered with high-pass filters of kernels $k = 3$ and $k = 7$, as defined in Eq. (8) and shown in Fig. 1.

As can be seen in Fig. 11, the high-pass filtering method can yield similar results as nonlinear filtering in the case of a kernel $k = 3$, which corresponds to strong filtering, showing that this phase standard deviation is obtained at the cost of a strong loss of spatial resolution. On the other hand, a weaker filtering ($k = 7$) does not significantly improve the standard deviation of the signal in comparison with linear filtering without any high-pass filtering. This result shows that the nonlinear filtering efficiently suppresses the zero-order term. It can indeed be assumed that the very strong high-pass filtering ($k = 3$)

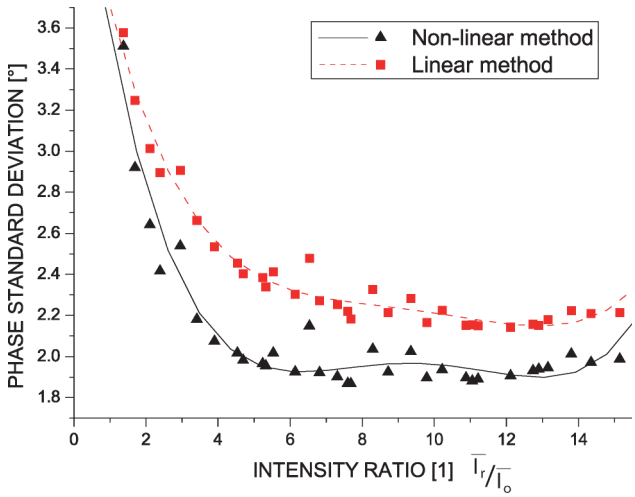

Fig. 10. (Color online) Phase standard deviation on the measured zone of Fig. 9(b) as a function of the mean intensity ratio between the reference and the object waves.

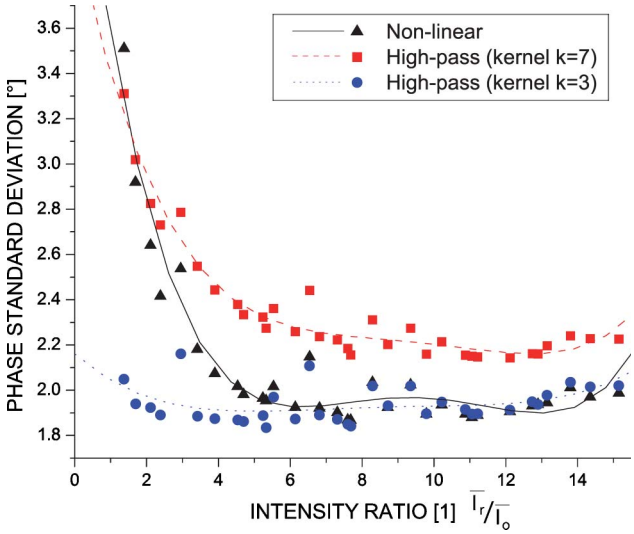

Fig. 11. (Color online) Phase standard deviation on the measured zone of Fig. 9(b) in comparison with the nonlinear technique with high-pass filters with different kernels as defined in Eq. (8).

suppresses the contributions of the dc term, so that only the intrinsic standard deviation from the light source and the sample remains. Therefore, it can be seen that the nonlinear method fully suppresses the numerical noise induced by the zero-order term to reach the minimum of experimental noise. These results also show that, since the intensity ratio is sufficient to fulfill the assumptions required by the algorithm, the optimum of reconstruction quality is reached without any need to finely tune this key parameter. This feature makes the technique rather flexible.

4. Conclusion

We have experimentally validated a new nonlinear reconstruction technique for digital holography. This technique proved to be efficient at suppressing the object autocorrelation, namely, the zero-order term. In addition, the new method does not require the use of a high-pass filter, which affects the resolution of the reconstructed wave field. We have also shown that it improves the resolution of the reconstruction, since a full quadrant of the Fourier spectrum can be used for recording, contrary to a fraction of it in the case of standard filtering. This leads to diffraction-limited imaging for digital holographic microscopy in the whole visible range, while retaining the one-shot feature of off-axis digital holographic microscopy.

This algorithm can be applied in standard experimental conditions. The only additional requirement is that the reference amplitude must be stronger than that of the object. Experiments showed that this algorithm is effective even in the case of a strong spectral overlap between the zero-order term and the diffraction orders or in nonideal measurement conditions; for example, in the case of an irregular space varying reference wave amplitude, provided that a simple calibration step is performed. This new

filtering method can be automated easily, since it does not require a manually specified window as in the standard Fourier techniques. The proposed method is therefore particularly suitable for measurements with low numerical apertures, where the overlap between various orders is inevitable, if one wants to keep the full resolution provided by the optical system. The image quality improvement can also be used for other recording conditions, since spectral overlap can also occur in the case of high magnification measurements.

N. Pavillon is supported by the Swiss National Science Foundation (SNSF) grant 205320-120118. The authors thank their colleagues in the MuVision Group, in particular, E. Shaffer and Y. Delacrétaz, and at Lyncée Tec SA (www.lynceetec.com) for their cooperation and several fruitful discussions.

References

1. C. S. Seelamantula, N. Pavillon, C. Depeursinge, and M. Unser, "Zero-order-free image reconstruction in digital holographic microscopy," in *IEEE International Symposium on Biomedical Imaging: from Nano to Macro* (IEEE, 2009), pp. 201–204.
2. J. W. Goodman and R. W. Lawrence, "Digital image formation from electronically detected holograms," Appl. Phys. Lett. **11**, 77–79 (1967).
3. U. Schnars and W. P. O. Jüptner, "Direct recording of holograms by a CCD target and numerical reconstruction," Appl. Opt. **33**, 179–181 (1994).
4. O. Coquoz, R. Conde, F. Taleblou, and C. Depeursinge, "Performances of endoscopic holography with a multicore optical fiber," Appl. Opt. **34**, 7186–7193 (1995).
5. J. Kühn, F. Charrière, T. Colomb, E. Cuche, F. Montfort, Y. Emery, P. Marquet, and C. Depeursinge, "Axial subnanometer accuracy in digital holographic microscopy," Meas. Sci. Technol. **19**, 074007 (2008).
6. P. Marquet, B. Rappaz, P. J. Magistretti, E. Cuche, Y. Emery, T. Colomb, and C. Depeursinge, "Digital holographic microscopy: a noninvasive contrast imaging technique allowing quantitative visualization of living cells with subwavelength axial accuracy," Opt. Lett. **30**, 468–470 (2005).
7. B. Kemper and G. von Bally, "Digital holographic microscopy for live cell applications and technical inspection," Appl. Opt. **47**, A52–A61 (2008).
8. E. Cuche, P. Marquet, and C. Depeursinge, "Simultaneous amplitude-contrast and quantitative phase-contrast microscopy by numerical reconstruction of Fresnel off-axis holograms," Appl. Opt. **38**, 6994–7001 (1999).
9. U. Schnars and W. P. O. Jüptner, "Digital recording and numerical reconstruction of holograms," Meas. Sci. Technol. **13**, R85–R101 (2002).
10. P. Picart and J. Leval, "General theoretical formulation of image formation in digital fresnel holography," J. Opt. Soc. Am. A **25**, 1744–1761 (2008).
11. D. Gabor, "A new microscopic principle," Nature **161**, 777–778 (1948).
12. E. N. Leith and J. Upatnieks, "Reconstructed wavefronts and communication theory," J. Opt. Soc. Am. **52**, 1123–1130 (1962).
13. M. Takeda, H. Ina, and S. Kobayashi, "Fourier-transform method of fringe-pattern analysis for computer-based topography and interferometry," J. Opt. Soc. Am. **72**, 156–160 (1982).
14. E. Cuche, F. Bevilacqua, and C. Depeursinge, "Digital holography for quantitative phase-contrast imaging," Opt. Lett. **24**, 291–293 (1999).
15. I. Yamaguchi and T. Zhang, "Phase-shifting digital holography," Opt. Lett. **22**, 1268–1270 (1997).
16. Y. Takaki, H. Kawai, and H. Ohzu, "Hybrid holographic microscopy free of conjugate and zero-order images," Appl. Opt. **38**, 4990–4996 (1999).
17. L. Cai, Q. Liu, and X. Yang, "Phase-shift extraction and wavefront reconstruction in phase-shifting interferometry with arbitrary phase steps," Opt. Lett. **28**, 1808–1810 (2003).
18. Z. Wang and B. Han, "Advanced iterative algorithm for phase extraction of randomly phase-shifted interferograms," Opt. Lett. **29**, 1671–1673 (2004).
19. P. Guo and A. Devaney, "Digital microscopy using phase-shifting digital holography with two reference waves," Opt. Lett. **29**, 857–859 (2004).
20. J.-P. Liu and T.-C. Poon, "Two-step-only quadrature phase-shifting digital holography," Opt. Lett. **34**, 250–252 (2009).
21. T. M. Kreis and W. P. O. Jüptner, "Suppression of the dc term in digital holography," Opt. Eng. **36**, 2357–2360 (1997).
22. C. Liu, Y. Li, X. Cheng, Z. Liu, F. Bo, and J. Zhu, "Elimination of zero-order diffraction in digital holography," Opt. Eng. **41**, 2434–2437 (2002).
23. M. Liebling, T. Blu, and M. Unser, "Complex-wave retrieval from a single off-axis hologram," J. Opt. Soc. Am. A **21**, 367–377 (2004).
24. E. Garbusi, C. Pruss, and W. Osten, "Single frame interferogram evaluation," Appl. Opt. **47**, 2046–2052 (2008).
25. N. Demoli, J. Mestrović, and I. Sović, "Subtraction digital holography," Appl. Opt. **42**, 798–804 (2003).
26. G.-L. Chen, C.-Y. Lin, M.-K. Kuo, and C.-C. Chang, "Numerical suppression of zero-order image in digital holography," Opt. Express **15**, 8851–8856 (2007).
27. Y. Zhang, G. Pedrini, W. Osten, and H. Tiziani, "Reconstruction of in-line digital holograms from two intensity measurements," Opt. Lett. **29**, 1787–1789 (2004).
28. J. Weng, J. Zhong, and C. Hu, "Digital reconstruction based on angular spectrum diffraction with the ridge of wavelet transform in holographic phase-contrast microscopy," Opt. Express **16**, 21971–21981 (2008).
29. T. Colomb, F. Montfort, J. Kühn, N. Aspert, E. Cuche, A. Marian, F. Charrière, S. Bourquin, P. Marquet, and C. Depeursinge, "Numerical parametric lens for shifting, magnification, and complete aberration compensation in digital holographic microscopy," J. Opt. Soc. Am. A **23**, 3177–3190 (2006).
30. E. Cuche, P. Marquet, and C. Depeursinge, "Spatial filtering for zero-order and twin-image elimination in digital off-axis holography," Appl. Opt. **39**, 4070–4075 (2000).
31. F. Montfort, F. Charrière, T. Colomb, E. Cuche, P. Marquet, and C. Depeursinge, "Purely numerical compensation for microscope objective phase curvature in digital holographic microscopy: influence of digital phase mask position," J. Opt. Soc. Am. A **23**, 2944–2953 (2006).
32. E. Cuche, P. Marquet, and C. Depeursinge, "Aperture apodization using cubic spline interpolation: application in digital holographic microscopy," Opt. Commun. **182**, 59–69 (2000).
33. F. Charrière, T. Colomb, F. Montfort, E. Cuche, P. Marquet, and C. Depeursinge, "Shot-noise influence on the reconstructed phase image signal-to-noise ratio in digital holographic microscopy," Appl. Opt. **45**, 7667–7673 (2006).